Analysis and design principles for shear-mode piezoelectric energy harvesting with ZnO nanoribbons

2010 Smart Mater. Struct. 19 055027

(http://iopscience.iop.org/0964-1726/19/5/055027)

Smart Mater. Struct. **19** (2010) 055027 (7pp) doi:10.1088/0964-1726/19/5/055027

Analysis and design principles for shear-mode piezoelectric energy harvesting with ZnO nanoribbons

C Majidi[1], M Haataja[2] and D J Srolovitz[3]

[1] School of Engineering and Applied Sciences (SEAS), Harvard University, Cambridge, MA 02138, USA
[2] Department of Mechanical and Aerospace Engineering, Program in Applied and Computational Mathematics (PACM), Princeton University, Princeton, NJ 08544, USA
[3] Institute of High Performance Computing, Agency for Science, Technology and Research (A*STAR), 138632, Singapore

E-mail: cmajidi@seas.harvard.edu

Received 17 July 2009, in final form 24 March 2010
Published 16 April 2010
Online at stacks.iop.org/SMS/19/055027

Abstract
A comprehensive theory addresses the potential for nanoscale energy harvesting with an array of vertically aligned zinc oxide (ZnO) nanoribbons. Through shear-mode piezoelectric coupling, the nanoribbons are capable of generating electricity from elastic deformations induced by sliding friction or mechanical vibration. In contrast to current ZnO nanowire generators, nanoribbons exhibit a unique combination of geometry and poling orientation that eliminates the need for a nanostructured cathode and allows electrodes to be permanently bonded to the array. The theory incorporates principles and design constraints from solid mechanics, electrostatics, piezoelectricity, vibration dynamics, circuit theory, and tribology. The accuracy of the approximate algebraic solutions is evaluated with finite element modeling. For geometries and operation modes of interest, the electrical power output and conversion ratio from mechanical power input are limited to $\sim$10 nW mm^{-3} and 1000:1, respectively. While modest, such numbers provide a proper perspective on the potential for nanopiezoelectric energy harvesting.

(Some figures in this article are in colour only in the electronic version)

1. Introduction

Nanopiezoelectric energy harvesting (NPEH) represents a new and potentially important branch of nanotechnology [1, 2]. One aim of NPEH is to embed materials, such as textiles [3], with nanosized generators that convert otherwise wasted mechanical energy into electricity. Another potential for NPEH is to allow nanoelectronic and nanoelectromechanical (NEMS) systems to be self-powered, analogous to the aim of piezoelectric energy harvesting for larger scale systems [4].

NPEH was recently reported with arrays of vertically aligned zinc oxide (ZnO) nanowires that convert sliding friction into electricity [5]. While this represents a promising first step, theory suggests that such a design may be improved by replacing the nanowires with *nanoribbons*. As illustrated in figures 1(a) and (b), ZnO nanoribbons [6, 7] are piezoelectrically poled along their thickness and so elastic deformation from interfacial sliding or vibration will induce an electric potential drop across the length. For an array of vertically aligned nanoribbons, electricity can be generated by simply placing electrodes on opposite sides of the array. In contrast, ZnO nanowires generate a potential drop across their thickness and so electric current can only be generated through a nanostructured electrode that allows tip contact without causing an electrical short [5].

In this paper we introduce a theoretical model that predicts the electrical power generated by an array of vertically aligned ZnO nanoribbons subject to either sliding friction or vibration. The magnitude of mechanical power input is constrained by the strength and excitation characteristics of the

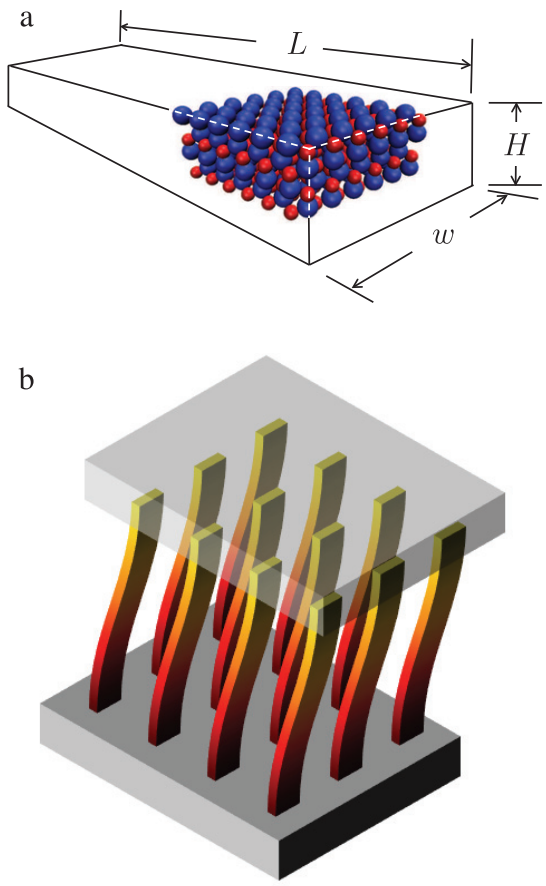

Figure 1. (a) ZnO nanoribbons have a wurtzite crystal lattice with piezoelectric poling through the thickness. They have a thickness $H \sim 10$ nm, width $w \sim 100$ nm, and length $L \sim 1$–100 μm. (b) An array of vertically aligned nanoribbons can convert elastic deformations from sliding friction or mechanical vibration into electricity. This is accomplished through shear-mode piezoelectric coupling, which induces a gradient in electric potential along the ribbon length.

nanoribbons. The proportion of mechanical power input that is converted to electrical power is controlled by geometry and the material constants for shear-mode piezoelectric coupling. These relationships are established through a comprehensive theory that incorporates continuum elasticity, piezoelectricity, vibration dynamics, circuit theory, and tribology. Approximate algebraic solutions to the governing equations are used to derive scaling laws and design criteria.

In addition to exploring the potential of ZnO nanoribbons for NPEH, this analysis addresses the more general topic of piezoelectric energy harvesting (PEH) through shear-mode piezoelectric coupling. Current methods for PEH use elongational e_{31} and e_{33} coupling to generate electricity from a bending cantilever [4]. These systems, however, require composites of two or more layers that are difficult to replicate with current vapor deposition techniques for single crystal nanostructures. With shear-mode coupling, lateral deformations can induce an electric potential drop across a single crystal. The dual to this mechanism had previously been explored with shear-mode actuators [8–10].

The system parameters and governing equations are presented in section 2 along with a comparison to the results of a finite element simulation. The theoretical results are used to predict the power output and performance of an array of nanoribbons subject to either sliding friction (section 3) or vibration (section 4). The paper closes with a brief discussion (section 5) and conclusion (section 6) that summarize the results and remark on their implications for NPEH.

2. Theory

ZnO nanoribbons are flat, ribbon-like, single crystals that have a thickness $H \sim 10$ nm, width $w \sim 100$ nm, and length $L \sim 1$–100 μm [6]. Because of the orientation of its wurtzite crystal lattice, a nanoribbon is piezoelectrically poled through its thickness.

As illustrated in figure 1(b), the nanoribbons form an array in which they are vertically aligned and spaced a distance ξ apart. When the array is dragged against a surface or mechanically vibrated, the ribbons will elastically deform in the lateral direction. Because the thickness H is typically an order of magnitude less than the width w, analysis will henceforth be limited to planar deformation along the thickness and width directions.

2.1. Kinematics

The unit vectors $\mathbf{e}_1$ and $\mathbf{e}_3$ are oriented along the length and thickness directions, respectively. In other words, $\{\mathbf{e}_1, \mathbf{e}_3\}$ form an orthonormal basis where $\mathbf{e}_3$ coincides with the e_{33} poling direction. Points in the ribbon are uniquely identified with their position $\mathbf{X} = x_1\mathbf{e}_1 + x_3\mathbf{e}_3$ in the undeformed configuration. Here, the coordinates x_1 and x_3 are defined on the intervals $[0,\ L]$ and $[-H/2,\ H/2]$, respectively.

Under mechanical loading, the ribbon deforms elastically to a final configuration $\mathbf{x} = \mathbf{X} + \mathbf{u}$, where $\mathbf{u} = u_1(x_1, x_3)\mathbf{e}_1 + u_3(x_1, x_3)\mathbf{e}_3$ is the displacement vector. Assuming small displacements, this corresponds to an elastic strain field

$$\boldsymbol{\gamma} = \tfrac{1}{2}\{\nabla\mathbf{u} + \nabla\mathbf{u}^{\top}\}, \tag{1}$$

which has components

$$\gamma_{11} = \frac{\partial u_1}{\partial x_1} \qquad \gamma_{33} = \frac{\partial u_3}{\partial x_3}$$
$$\gamma_{13} = \frac{1}{2}\left(\frac{\partial u_1}{\partial x_3} + \frac{\partial u_3}{\partial x_1}\right). \tag{2}$$

2.2. Constitutive laws

For a piezoelectric material, the second-order strain tensor $\boldsymbol{\gamma}$ is coupled to the second-order stress tensor $\mathbf{T}$, electric field vector $\mathbf{E}$, and electric displacement vector $\mathbf{D}$. Mathematically, these relationships are expressed through the following constitutive laws [11]:

$$\mathbf{T} = \mathbf{C}{:}\boldsymbol{\gamma} - \mathbf{E}\cdot\mathbf{e} \qquad \mathbf{D} = \mathbf{e}{:}\boldsymbol{\gamma} + \boldsymbol{\varepsilon}\cdot\mathbf{E}. \tag{3}$$

Here, **C** is the fourth-order stiffness tensor, **e** is the third-order piezoelectric coupling tensor, and $\boldsymbol{\varepsilon}$ is the second-order electric permittivity tensor.

In the $\mathbf{e}_1$–$\mathbf{e}_3$ plane, the constitutive laws can be expressed in the following indicial form:

$$T_{11} = C_{11}\gamma_{11} + C_{13}\gamma_{33} - e_{31}E_3 \tag{4}$$

$$T_{33} = C_{13}\gamma_{11} + C_{33}\gamma_{33} - e_{33}E_3 \tag{5}$$

$$T_{13} = 2C_{44}\gamma_{13} - e_{15}E_1 \tag{6}$$

$$D_1 = 2e_{15}\gamma_{13} + \varepsilon_{11}E_1 \tag{7}$$

$$D_3 = e_{31}\gamma_{11} + e_{31}\gamma_{33} + \varepsilon_{33}E_3. \tag{8}$$

For ZnO, $C_{11} = 210$ GPa, $C_{13} = 105$ GPa, $C_{33} = 210$ GPa, $C_{44} = 42.5$ GPa, $e_{31} = -0.61$ C m^{-2}, $e_{33} = 1.14$ C m^{-2}, $e_{15} = -0.59$ C m^{-2}, and $\varepsilon_{11} = \varepsilon_{33} = 7.38\times10^{-11}$ F m^{-1} [11].

Of particular interest is the change in electric potential $\Phi = \Phi(x_1, x_3)$ along the length of the ribbon. The x_1-component of the electric field is defined as $E_1 = -\partial\Phi/\partial x_1$ and so the potential difference across the two ends of the ribbon is approximately $\Delta\Phi = -E_1 L$.

2.3. Balance laws

Lateral deformation is controlled by a shear force $V\mathbf{e}_3$ and bending moment M exerted on the tip of each ribbon. The externally applied shear force must be balanced by the internal shear stress T_{13}, which has an average value of $\tau_0 = V/wH$.

In the absence of surface and space charge, the electric displacements D_1 vanishes, i.e. $D_1 = 0$. Therefore, the constitutive equations (6) and (7) imply

$$\tau_0 = -\left\{e_{15} + \frac{\varepsilon_{11}C_{44}}{e_{15}}\right\}E_1. \tag{9}$$

Noting that $\tau_0 = V/wH$ and $E_1 = -\Delta\Phi/L$, it follows that the difference in electric potential across the two ends of the sheared ribbon is approximately

$$\Delta\Phi = \frac{VL}{wH}\left\{e_{15} + \frac{\varepsilon_{11}C_{44}}{e_{15}}\right\}^{-1}. \tag{10}$$

2.4. Computational validation

In figure 2(a), the algebraic estimate for $\Delta\Phi$ is compared with the results of a finite element simulation. Referring to figure 2(b), a three-dimensional finite element analysis is performed on a five-layer ≈15 400 element mesh in COMSOL Multiphysics 3.4 (COMSOL AB, 2007). One end of the ribbon is kinematically constrained and electrically ground while the opposite end is subject to a shear force V uniformly distributed by a shear traction V/wH over the surface.

The non-uniform shear stress distribution leads to a non-uniform electric potential field along the width and thickness. Nonetheless, the total drop in potential $\Delta\Phi$ across the two ends of the ribbon is consistent with the theoretical approximation based on the average shear stress $\tau_0 = V/wH$. Moreover, the plane stain assumption of restricting deformation to $\mathbf{e}_1$–$\mathbf{e}_3$ also appears to be valid.

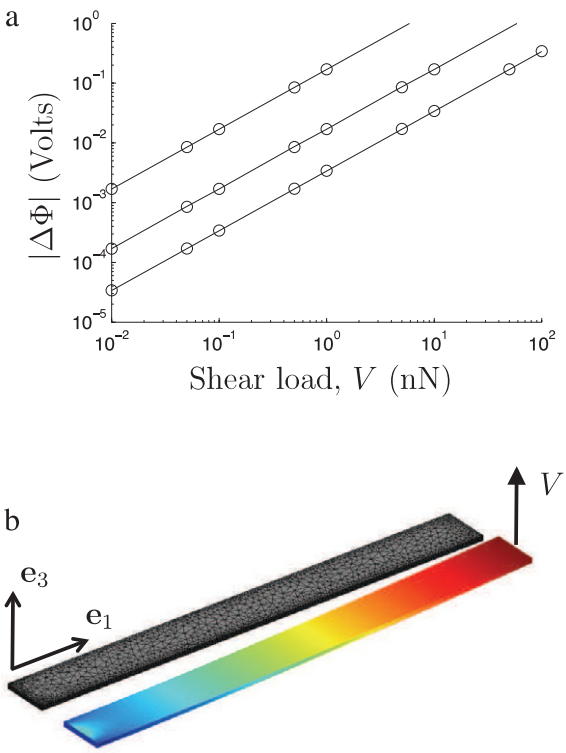

Figure 2. Comparison of algebraic solution (solid line) and finite element simulation (open circles) for the drop in electric potential $\Delta\Phi$ across the length of the ribbon as a function of applied shear force V. (a) Top curve: $L = 1$ μm, $H = 10$ nm, $w = 100$ nm; middle curve: $L = 10$ μm, $H = 100$ nm, $w = 1$ μm; bottom curve: $L = 1$ μm, $H = 100$ nm, $w = 0.5$ μm. (b) Finite element mesh and electric potential field of a ribbon ($L = 10$ μm, $H = 100$ nm, $w = 1$ μm) subject to a 5 nN shear load. The ribbon is electrically ground at the fixed end.

3. Sliding friction

The mechanical work performed on the ribbon during sliding has the form

$$W = \frac{2L^3V^2}{YwH^3}, \tag{11}$$

where $Y = C_{11} - C_{13}^2/C_{33}$ is Young's modulus for plane stress. In contrast, the total electrostatic energy stored in the crystal is

$$U = \frac{\varepsilon_{11}wH\Delta\Phi^2}{2L} = \frac{\varepsilon_{11}LV^2}{2wH}\left\{e_{15} + \frac{\varepsilon_{11}C_{44}}{e_{15}}\right\}^{-2}. \tag{12}$$

The conversion ratio is defined as $\chi = U/W$ and indicates the proportion of mechanical energy or power that can be converted into electricity:

$$\chi = \frac{\varepsilon_{11}YH^2}{4L^2}\left\{e_{15} + \frac{\varepsilon_{11}C_{44}}{e_{15}}\right\}^{-2}. \tag{13}$$

Interestingly, the conversion ratio is invariant to the magnitude of the shear force and is instead inversely proportional to the aspect ratio squared. This suggests that the efficiency of conversion from mechanical power input to electrical power output does not scale with length but instead scales with the aspect ratio and is greatest for low aspect ratio ribbons.

Inserting the piezoelectric constants for ZnO into equation (13), the conversion ratio becomes

$$\chi = 0.083\left(\frac{H}{L}\right)^2. \tag{14}$$

Hence, even for low aspect ratio ribbons with $H = 0.1L$, the conversion ratio will only be less than a tenth of a per cent.

In addition to the modest conversion ratio, power output is limited by the maximum shear force V that can be exerted on the individual tips. In general, V will be limited by the fracture strength of the ribbon as well as the shear strength of the sliding interface. These constraints are discussed in greater detail in appendix A. In the case of friction-limited shear, the maximum electrostatic energy that can be stored in a ribbon is approximately

$$U_0 = 0.021\mu\frac{\varepsilon_{11}Y^2wH^5}{L^3}\left\{e_{15}+\frac{\varepsilon_{11}C_{44}}{e_{15}}\right\}^{-2}, \tag{15}$$

where μ is the coefficient of friction between the ZnO tip and contacting substrate. For typical values of $\mu = 0.3$, $H = 10$ nm, $w = 100$ nm, $L = 1$ μm, this corresponds to $U_0 = 3.3 \times 10^{-21}$ J. Hence, for a 1 mm^2 array of ribbons spaced $\xi = 100$ nm apart and dragged at a rate of 1 m s^{-1}, the total power output is 0.33 nW.

4. Mechanical vibration

In the case of mechanical vibration, the tip of the ribbon is permanently bonded to an electrode. Therefore, in addition to inducing a shear force V, mechanical excitation will also induce a bending moment that prevents the tip from rotating.

Just as with frictional loading, shear-mode piezoelectric coupling will convert the vibration-induced lateral deformations into electricity. As each individual ribbon vibrates back and forth with a frequency ω, the electrical current alternates in direction. This produces AC power that can then be rectified to charge a battery or power a host system.

As with other vibrational piezoelectric energy harvesting devices, the AC power output P is greatest when the ribbons are excited at their natural resonant frequency ω_n. In general [12],

$$P \approx P_0\left\{1+\left(\frac{\omega-\omega_n}{\zeta\omega_n}\right)^2\right\}^{-1}. \tag{16}$$

Here, P_0 is the AC power output at resonance and ζ is the damping ratio. This formula suggests that a larger damping ratio ζ allows energy harvesting over a broad range of excitation frequencies.

Ignoring the mass of the ribbon itself, the natural frequency ω_n of an individual ribbon has the form $\omega_n = \sqrt{k_m/m}$. Here

$$k_m = \frac{YwH^3}{L^3} \tag{17}$$

is the lateral stiffness, $m = \rho\xi^2\ell$ is the portion of the mass of the bonded electrode that is supported by the individual ribbon, ρ is the electrode density, and ℓ is the electrode thickness. However, depending on the orientation of the array, mass m may also be limited by the buckling strength ($\pi^2YwH^3/12gL^2$, where g is gravity) or fracture strength of the ribbon ($m = S_U wH/g$, where S_U is the ultimate tensile strength and is typically on the order of 1 GPa).

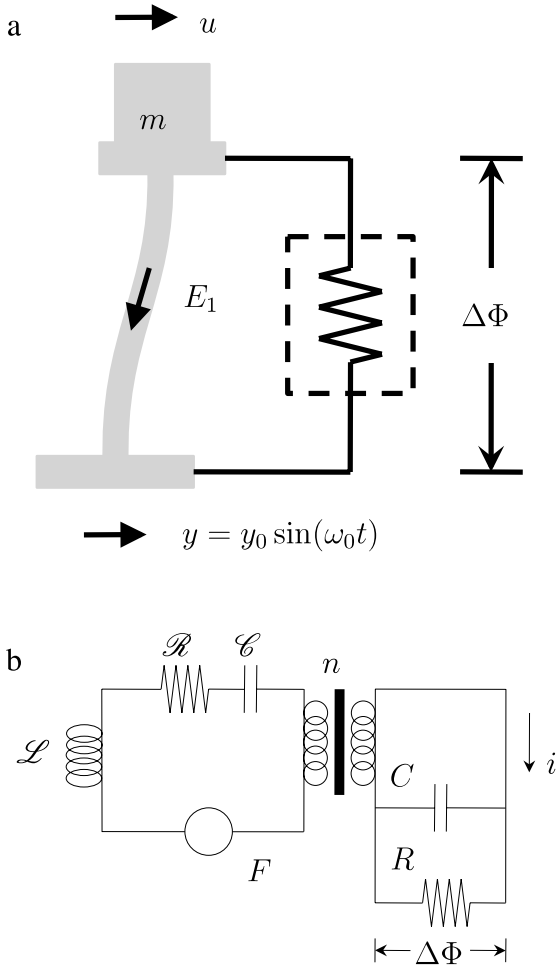

Figure 3. Equivalent circuit representation of a piezoelectric cantilever connected to a battery [13].

4.1. AC power output

The resonant power output of an individual cantilever is determined with an equivalent circuit model that addresses both the static and dynamical effects of elastic deformation, piezoelectric coupling, electricity storage, and energy dissipation [13]. The equivalent circuit representation of the cantilever, electrode, and battery is presented in figure 3.

Definitions for each element and the governing equations for the complete circuit are presented in appendix B. The governing equations are used to determine the potential drop $\Delta\Phi$ during resonance. This corresponds to an AC power $P_0 = |\Delta\Phi|^2/2R$, where R is the electrical resistance of the charging battery or host electronics.

Following the same steps as in [13], the governing equations (B.2) and (B.3) are used to estimate the power output at resonance:

$$P = R(k_m e_{15}\omega_n y_0)^2\{8(\zeta C_{44})^2[1+(RC\omega_n)^2] + 8ne_{15}R\omega_n\zeta C_{44} + 2(ne_{15}R\omega_n)^2\}^{-1}. \quad (18)$$

Here, $n = e_{15}wH/L$ is the equivalent turns ratio, $C = \varepsilon_{11}wH/L$ is the capacitance of the ribbon, $\zeta = b/2m\omega_n$ is the dimensionless damping ratio, and the acceleration $y_0\omega_n^2$ corresponds to the Laplacian of the input vibration [13].

4.2. Design criteria

In order for substantial AC power to be harvested, the nanoribbon array must resonate within the range of anticipated excitation frequencies. In most buildings, machinery, and civil infrastructure, ambient vibrations are typically on the order of 1–100 Hz. To be compatible with such a low driving frequency, each nanoribbon must have a high aspect ratio. However, as shown in equation (14), the conversion ratio decreases significantly with increased aspect ratio. Nonetheless, for a prescribed driving frequency ω_0, the condition $\omega_n = \omega_0$ requires the ribbon to have a length

$$L = H\left\{\frac{Yw}{\omega_0^2\rho\xi^2\ell}\right\}^{1/3}. \quad (19)$$

Design is also constrained by the maximum allowable vibrational amplitude u_0. As with frictional loading, the ribbons will break if sheared beyond their fracture strength. This occurs when $u_0 = \gamma_0 L^2/6H$, where γ_0 is the ultimate tensile strength of the crystal. Because the ribbons are virtually inextensible, amplitude is also limited by the natural length of the ribbon. For moderate lateral displacements where the center of the ribbon rotates by 30°, this corresponds to approximately $u_0 = (4L/\pi)(1-\sqrt{3}/2)$.

Driving the base of the cantilever by a displacement $y = y_0\sin(\omega_0 t)$ will cause the system to asymptotically reach a maximum tip displacement on the order of $y_0/2\zeta_0$. Therefore, the vibration amplitude must be less than the critical value $2\zeta_0 u_0$. Assuming that the ribbons are sufficiently thin to avoid brittle fracture in bending, y_0 is bounded above by

$$y_0 = \frac{8\zeta_0 L}{\pi}\left(1-\frac{\sqrt{3}}{2}\right). \quad (20)$$

Substituting in the expressions for L and y_0 and solving $\mathrm{d}P/\mathrm{d}R = 0$ implies that P is at an extreme value when R equals

$$R^* = \frac{2C_{44}\zeta_0}{\sqrt{(2\zeta_0 C_{44}\varepsilon_{11})^2 + e_{15}^4}}\left(\frac{Y}{\omega_0^5\rho\xi^2\ell w^2}\right)^{1/3}. \quad (21)$$

Substituting this into P yields an expression for the AC power generation of each cantilever. Multiplying by $(\ell/\xi)^2$ gives the total power output of the array:

$$\mathscr{P} = \frac{2(2-\sqrt{3})^2 e_{15}^2 H^2\rho\ell^3\omega_0^3 Y\zeta_0}{\pi^2 C_{44}\left(\sqrt{(2\zeta_0 C_{44}\varepsilon_{11})^2 + e_{15}^4} + e_{15}^2\right)}. \quad (22)$$

From equation (22) it is apparent that the total power output increases with increasing thickness H, resonant frequency ω_0, device dimension ℓ, and damping ratio ζ_0. The increasing power output with increasing damping ratio is counter-intuitive and comes from the condition that greater ζ_0 allows for a greater vibrational amplitude y_0.

4.3. Example

Suppose that the nanoribbon array is supporting a gold electrode ($\rho = 20\times10^3$ kg m^{-3}). Moreover, assume that the complete system occupies a volume ℓ^3 with $\ell = 1$ mm, comparable to the size of existing MEMS-based energy harvesting systems. The total power output $\mathscr{P}$ is calculated for a prescribed resonant frequency $\omega_0 = 10$ kHz and damping ratio $\zeta_0 = 1$, which implies that the system is critically damped. For a ribbon of thickness $H = 0.1$ μm it follows from equation (22) that the total AC power output will be $\mathscr{P} = 0.6$ nanowatts (nW). Furthermore, if we prescribe a width $w = 5H = 0.5$ μm and spacing $\xi = 10H = 1$ μm, then it follows that the ribbon should have a length $L = 33$ μm and vibrate with an amplitude $y_0 = 11$ μm at the base.

Another important design parameter is the required battery resistance R^*. According to equation (21), $R^* = 9\times10^{14}$ Ω, which will result in an internal electric field of $E_1 = 30$ MV m^{-1}. This is of the order of the dielectric strength of a semiconductor and suggests that electric breakdown could occur. Setting $R = 10^{13}$ Ω decreases E_1 to 0.5 MV m^{-1}, well below the threshold for electric breakdown, but causes $\mathscr{P}$ to reduce to 12 picowatts (pW).

5. Discussion

ZnO nanostructures have received considerable attention and publicity for their potential role in energy harvesting. In contrast to MEMS-based systems, ZnO nanostructures allow piezoelectric energy harvesting at the nanometer scale and thus provide a unique opportunity for self-powered nanoelectronics and NEMS. Moreover, because of their simple, single crystal structure, these NPEH systems can be produced with existing fabrication techniques [3, 5–7].

Elastic rod theory and piezoelectric modeling are used to evaluate the ability of an array of vertically aligned ZnO nanoribbons to convert elastic deformation into electrical power. Deformation is induced by sliding friction or mechanical vibration and generates electricity through shear-mode piezoelectric coupling.

The theory suggests that an array of vertically aligned ZnO nanoribbons can produce as much as 1 nW mm^{-2} and 1–100 nW mm^{-3} electricity. While adequate to run a low power device such as a 30 pW processor [14], these estimates are significantly less than the power density of MEMS-based systems of comparable size (0.1–1 μW mm^{-3} [4, 15]). In addition to the relatively low power output, the theory also predicts a low ratio for the conversion of mechanical power input to electricity output.

6. Concluding remarks

Progress in nanoscale piezoelectric energy harvesting (NPEH) will require design innovations that improve the power output

density and power conversion ratio. Theoretical estimates for vertically aligned ZnO nanoribbons suggest only modest power generation. This is due to the small size scale, high aspect ratio, and dependency on shear-mode (e_{15}) piezoelectric coupling. Future efforts in NPEH should explore alternative geometries and methods that, for example, exploit elongational (e_{31} and e_{33}) coupling.

Acknowledgments

The authors wish to thank Professors Romesh Batra and Dan Inman (Virginia Tech) for their helpful remarks and suggestions.

Appendix A. Shear strength of a nanoribbon array

When the array is dragged across a smooth surface, the tips of the ribbons are loaded with a shear force V. As demonstrated in equation (10), greater shear load results in a greater difference in electric potential. However, the magnitude of the shear force will be limited by the shear strength of the sliding interface as well as the fracture strength of the ribbon.

The interfacial shear strength is expected to be controlled by a combination of friction and adhesion. Friction will be limited by the coefficient of friction μ and the maximum axial load F_0 that can be exerted on the ribbon prior to buckling. This corresponds to an interfacial force of

$$V_{\mathrm{f}} = \mu F_0 = \mu \frac{\pi^2 Y w H^3}{48 L^2}. \tag{A.1}$$

For typical values of $\mu = 0.3$, $H = 10$ nm, $w = 100$ nm, $L = 1$ μm, the critical shear strength is estimated to be $V_{\mathrm{f}} = 1.2$ nN. This value may be further enhanced by adhesion, which may arise from electrostatic, capillary, or van der Waals interactions.

The mechanisms for brittle fracture are quite complex, and so it is difficult to establish a reliable estimate for the true fracture strength of the ribbon. Nonetheless, conventional elastic rod theory does furnish an upper bound on the fracture strength that will be useful at this stage of design. It suggests that fracture will begin when increasing shear load causes the induced strain to reach the ultimate tensile strain γ_{t} of the crystal. The induced strain is greatest inside the fixed base of the ribbon, where the shear force exerts a bending moment VL on the cross section. At the tensile edge of the cross section, the strain is approximately $\gamma_{11} = 6VL/YwH^2$. This implies that failure occurs when V reaches the critical value

$$V_0 = \frac{YwH^2\gamma_{\mathrm{t}}}{6L}. \tag{A.2}$$

For crystalline material like ZnO, γ_{t} is expected to be less than 0.01. Again assuming $H = 10$ nm, $w = 100$ nm, $L = 1$ μm, it follows that $V_0 = 35$ nN. Although this is greater than V_{f}, it is possible for V_0 to be the smaller of the two upper bounds when the aspect ratio L/H is smaller.

Appendix B. Equivalent circuit model

In the equivalent circuit model, the inductance $\mathscr{L}$ corresponds to the mass m, the resistance $\mathscr{R}$ replaces the mechanical damping coefficient b, and the capacitance $\mathscr{C}$ equals the inverse of the mechanical stiffness k_{m} of the cantilever. The parameter n represents the ratio of the number of turns in the equivalent transformer between the mechanical and electrical portions of the system and is associated with the piezoelectric coupling between the shear load V and voltage drop $\Delta\Phi$. Lastly, C and R represent the capacitance and resistance of the cantilever and battery, respectively.

By linear superposition, a prescribed lateral tip displacement u and potential drop $\Delta\Phi$ will induce the following shear force:

$$V = k_{\mathrm{m}} u + n\Delta\Phi, \tag{B.1}$$

where $k_{\mathrm{m}} = YwH^3/L^3$ is the lateral stiffness and $n = e_{15}wH/L$ is the turns ratio. The electrical current is $i = wH\dot{D}$, where D is the electric displacement along the $\mathbf{e}_1$ direction when the internal electric field is zero [13]. In this case, the average shear stress is $T_{13} = k_{\mathrm{m}}u/wH$ and so from the constitutive equations, $D = e_{15}k_{\mathrm{m}}u/C_{44}wH$, which implies $i = (e_{15}k_{\mathrm{m}}/C_{44})\dot{u}$ (the dot denotes the time derivative).

The base of the cantilever array is subject to a lateral displacement $y = y(t)$, which is a function of time t. In the case of uniform, periodic vibrations, $y(t)$ has the form $y = y_0 \sin(\omega t)$, where y_0 and ω are the amplitude and frequency of the vibrational motion. Vibrating the base induces a relative tip displacement $u = u(t)$ and an absolute tip displacement $y + u$. Performing a linear force balance on the supported mass yields $-V = m(\ddot{y} + \ddot{u})$. Adding damping and substituting in the equivalent circuit terms for the mechanical parameters yields the governing equation for an equivalent transformer:

$$my_0\omega_0^2 \sin(\omega_0 t) = \mathscr{L}\ddot{u} + \mathscr{R}\dot{u} + \frac{1}{\mathscr{C}}u + n\Delta\Phi \tag{B.2}$$

and

$$i = C\Delta\dot{\Phi} + \frac{1}{R}\Delta\Phi. \tag{B.3}$$

References

[1] Wang Z L 2007 The new field of nanopiezotronics *Mater. Today* **10** 20–8
[2] Wang Z L 2008 Self-powered nanotech *Sci. Am.* **298** 82–7
[3] Qin Y, Wang X and Wang Z L 2008 Microfibre–nanowire hybrid structure for energy scavenging *Nature* **451** 809–13
[4] Anton S R and Sodano H A 2007 A review of power harvesting using piezoelectric materials (2003–2006) *Smart Mater. Struct.* **16** R1–21
[5] Wang Z L and Song J 2006 Piezoelectric nanogenerators based on zinc oxide nanowire arrays *Science* **312** 242–5
[6] Pan Z W, Dai Z R and Wang Z L 2001 Nanobelts of semiconducting oxides *Science* **291** 1947–9
[7] Wei Y, Ding Y, Li C, Xu S, Ryo J-H, Dupuis R, Sood A K, Polla D L and Wang Z L 2008 Growth of vertically aligned ZnO nanobelt arrays on GaN substrate *J. Phys. Chem.* C **112** 18935–7
[8] Sun C T and Zhang X D 1995 Use of thickness-shear mode in adaptive sandwich structures *Smart Mater. Struct.* **4** 202–6

[9] Aldraihem O J and Khdeir A A 2000 Smart beams with extension and thickness-shear piezoelectric actuators *Smart Mater. Struct.* **9** 1–9
[10] Vel S S and Batra R C 2001 Exact solution for the cylindrical bending of laminated plates with embedded piezoelectric shear actuators *Smart Mater. Struct.* **10** 240–51
[11] Ding H J and Chen W Q 2001 *Three Dimensional Problems of Piezoelasticity* (Huntington, NY: Nova Science) p 7
[12] Siebert W M 1986 *Circuits, Signals, and Systems* (Cambridge, MA: MIT Press) p 113
[13] Roundy S and Wright P K 2004 A piezoelectric vibration based generator for wireless electronics *Smart Mater. Struct.* **13** 1131–42
[14] Seok M, Hanson S, Lin Y-S, Foo Z, Kim D, Lee Y, Liu N, Sylvester D and Blaauw D 2008 The Phoenix processor: a 30 pW platform for sensor applications *IEEE Symp. on VLSI Circuits* pp 188–9
[15] duToit N E and Wardle B L 2007 Performance of microfabricated piezoelectric vibration energy harvesters *Integr. Ferroelectr.* **83** 13–23